ISSN 1590-8844
International Journal of Mechanics and Control, Vol. 17, No. 01, 2016

NEURAL NETWORK DESIGN FOR INCIPIENT FAILURE DETECTION ON AIRCRAFT EM ACTUATOR

Matteo D. L. Dalla Vedova Davide De Fano Paolo Maggiore

Politecnico di Torino, Department of Aerospace Engineering, Corso Duca degli Abruzzi, 24 - 10129 Torino, Italy

ABSTRACT

Electro-Mechanic actuators are usually driven by Brushless-DC motors. Those ones can be affected by damages caused by fatigue and usage. At incipient stage, failures like partial short-circuit and rotor static eccentricity do not influences overall actuator performance, causing however oscillations in speed and command signals. Focusing on these oscillations, which presents periodic behaviour over the rotor revolution, neural networks are designed and trained to detect and quantify the damage entity. A different approach to this problem is performed, ignoring electrical measures of phase currents and potential drops, which are usually noisy and hardly available as actuator output. Classification results shows good performance in every speed-torque combination, reducing undetected failures and being capable to distinguish between the two kids of failures implemented.

Keywords: ANN, Prognostic, EMA, Short-circuit, Rotor Eccentricity

1 INTRODUCTION

Electro-Mechanic-Actuators(EMA) are one of the most common types of augmented flight control systems in fly-by-wire architectures. Especially for primary FCS, duty cycles are very difficult to predict, standing to the mission-user combination. This difficulty leads the research on components reliability and maintainability, in order to optimise procedures, reducing MTBF and MDT. In this scenario, prognostic studies results fundamental in order to reduce maintenance costs for preserving safety. Differently from mechanical fatigue, which can be predicted with a certain confidence level, electrical failures related to actuators, like partial short-circuit and rotor unbalancing, are hard to detect by the means of an external analysis. Those are mostly caused by extraordinary causes like current peaks or unexpected stresses, and consequences are undetectable in a large scale, as system performance and response could remain almost constant, while the initial incipient damage could rapidly degrades into a severe damage which compromise the system correct working, causing the actuator failure. Considering approximated models for incipient partial phase short circuit and static rotor unbalance damages, a mathematical model of an EMA in failure conditions is simulated, with the purpose of capturing damage-caused dynamics in the actuator output.

Contact author: Matteo D. L. Dalla Vedova

E-mail: matteo.dallavedova@polito.it

As the nature of the problem itself results highly nonlinear and non-fully deterministic, the adoption of Artificial Neural Networks is considered. Designing an appropriate architecture, ANN permits to detect also incipient failures with a good uncertainty level, also with a limited set of inputs, coming directly from noisy sensors. Therefore, the purpose of this work so is to develop a network architecture which takes as input typical system outputs and classifies them in order to detect failures and classifies them, reducing data size and data pre-processing phase, in order to perform a real-time classification.

2 EMA NUMERICAL MODEL

As previously mentioned, the goal of this research is the proposal of a new technique able to identify precocious symptoms (usually defined as failure precursors) of EMA degradations.

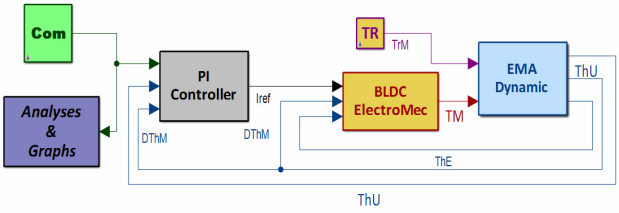

Figure 1 EMA Reference Model.

In order to assess the feasibility, the performance and the robustness of the aforesaid technique, a suitable simulation test bench has been developed in MATLAB/Simulink®. This numerical model, that is widely described in [1], is coherent with the considered EMA architecture shown in Fig. 1:

1. *Com*: generates input position commands.
2. *PI Controller*: simulates the actuator control electronics, closing position and speed feedback loops in and computing as output the reference current *Iref*.
3. *BLDC EM Model*: simulates the power drive electronics trough a SimScape model and the trapezoidal BLDC electromagnetic behaviour, evaluating torque developed as a function of three-phase current generated by an ideal H-bridge regulator.
4. *EMA Dynamic Model*: resolves the dynamic equation of mechanical behaviour by means of a 2 degree-of-freedom (d.o.f.) dynamic system.
5. *TR*: input block simulating the aerodynamic torques acting on the moving surface controlled by the actuator.
6. *Analyses & Graphs*: subsystem containing the EMA monitoring system.

It is useful to remark that this numerical model is able to simulate the dynamic behaviour of the considered EMA servomechanism taking also into account the effects of BLDC motor non-linearities [2-6], end-of-travels, compliance and backlashes acting on the mechanical transmission [7], analogic to digital conversion of the feedback signals, electrical noise acting on the signal lines and electrical offset of the position transducers [8] and dry friction (e.g. acting on bearings, gears, hinges and screw actuators) [9].

2.1 FAILURES IMPLEMENTATION

The present work is focused on two typical BLDC motor failures: the coil short-circuits (SC) and the bearing wear generating rotor static eccentricity (RE). Those are notable examples of progressive failures. At initial stage, those kinds of failures do not influence overall actuator performance substantially and the characteristics of the mechanical transmission, in terms of inertia, dry and viscous frictions, backlashes, noises, etc., could disguise or mitigate the failure effects. In these cases the analysis of electrical harmonics (e.g. phase currents) usually provides a better understanding of the failure progression and its estimation. One hidden aim of this work is to neglect electrical measures and harmonics analyses, focusing on speed and control signal oscillation over an entire rotor revolution. Short-circuit fault can actually occur within a coil, between two coils of the same phase, and two different phases: given that the first case is the most common and is the only one which permits the motor to continue working in degraded conditions. It also generally occurs first and will be the only case considered in this paper. According to [1], for simplicity is assumed that each phase winding consists of turns connected in series and the three-phase windings are wye-connected with a floating neutral point.

Three-phase windings with inter-turn fault in the *a*-phase winding is shown in Figure 3, where *as1* and *as2* represent the healthy and the damaged turns respectively, *ia* is the *a*-phase current, *if* is the circulating current in the shorted turns and *Zf* represents the possible external impedance between the shorted turns [10]. Short-circuits usually start between a few turns.

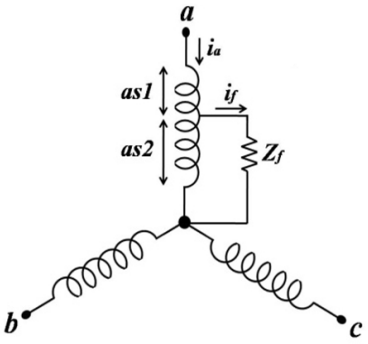

Figure 2 Schematic of turn-to-turn coil short circuit [11].

As in short-circuited resistance decreases, the resulting current increases, generating a localized temperature rising in the conductor which degrades the insulating paint, favours the extension of the failure to adjacent coils.
Considering previous hypothesis, this damage is implemented through an *integrity factor*, computed as follow:

$$N_{ph} = \frac{as2}{(as1+as2)} \qquad 0{,}75 \leq N_{ph} \leq 1 \tag{1}$$

This factor is bounded downward to 0.75, in order to guarantee hypothesis validity and incipient failure stage.
The modification of electrical impedance is so implemented through the following:

$$R_{ph} = R_0 \cdot N_{ph} \tag{2}$$

$$L_{ph} = \frac{L_0}{2 \cdot {N_{ph}}^2} \tag{3}$$

Rotor static eccentricity consists in a misalignment between its rotation axis and the stator axis of symmetry. It occurs usually due to tolerances and imperfections introduced during motor construction or to gradual increase of wear of the rotor shaft bearings. Whenever it occurs, the motor, supposed to have more than one polar couple, generates a periodically variable magnetic flux, as the air gap varies during rotation (Fig. 3) as a function of the rotor position θ:

$$g(\theta) = g_0(1 + \zeta \cos(\theta)) \quad \textit{where} \quad \zeta = \frac{x_0}{g_0} \tag{4}$$

In (4) RE is normalised to the nominal air-gap value g_0.
Considering performances, as reported in [12], output torque is lowered at same phase current condition respect to nominal, whereas, spectral analysis reveals the presence of sub-harmonics increasing with eccentricity.

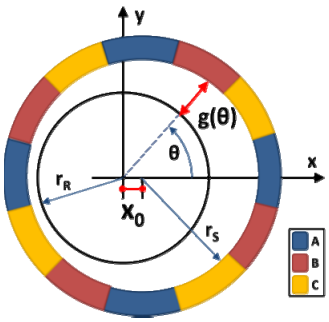

Figure 3 Schematic static RE.

RE and SC effects is by means of a simplified numerical algorithm, as both change the magnetic coupling between stator and rotor, in fact, failures can be modelled by proper static gains and angular modulations of the back-EMF coefficients:

$$\theta_e = 2\theta mod(360) \quad where \quad \varphi_{ph} = \begin{cases} 0° \\ 120° \\ 240° \end{cases} \tag{5}$$

$$K_{ph} = K(\theta_e) \cdot N_{ph} \cdot \left(1 + \zeta cos\left(\theta_e + \varphi_{ph}\right)\right) \tag{6}$$

The effects that these progressive failures produce on the dynamic behaviours of the considered actuation system are discussed in [1].

3 NEURAL NETWORK INPUT BUILDING

Three simulation campaigns were performed, to analyse single failure behaviour for RE and SC, then a multiple failures combination. Every simulation presents a constant speed command with fixed values of resistant torque and damage entity. Initial condition for every simulation is actuator settled in neutral position.
The principal hypothesis for simulations is that phase currents would not reach the maximum value of 22.5A, so that *PI controller* is not saturated. In order to assure this, a characterisation of the actuator were performed, finding the extreme working line at maximum current conditions.

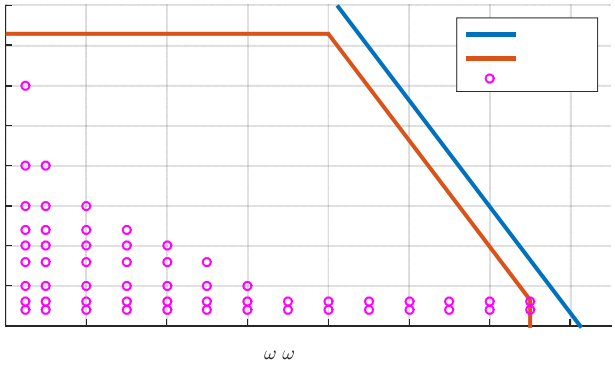

Figure 4 Simulation grid & boundaries.

Simulation grid is shaped to cover typical actuator working conditions, featured by low torque and high speeds. The considered output were the rotor speed and the reference signal coming from the controller.

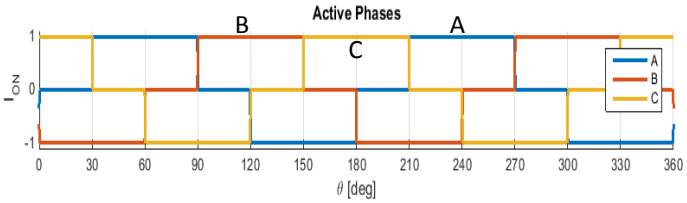

Figure 5 H-bridge switching sequence.

4 SHORT CIRCUIT OUTPUT ANALYSES

For the output analyses, a rotated reference system is introduced to match the x axis with the boundary point between two A and B phases windings. Doing so, it is possible to divide an entire revolution in twelve sectors corresponding to the stator windings.

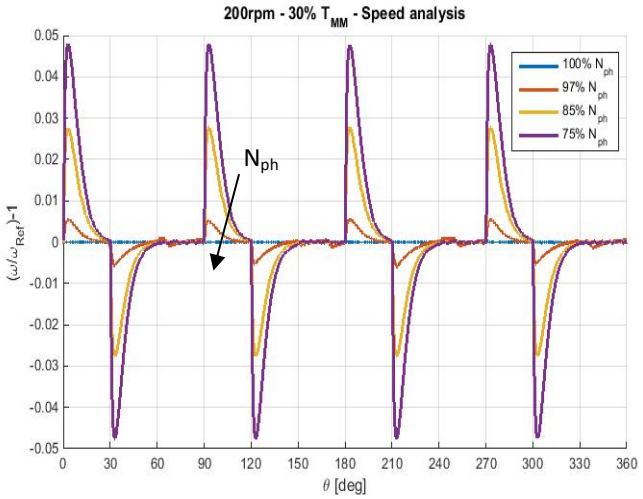

Figure 6 Speed response at various SC conditions.

To emphasise oscillations, as in Figure 6, signals are normalised to the average value for the entire rotation.

$$\hat{X}(\theta) = \frac{X(\theta)}{X_{360}} - 1 \tag{7}$$

Considering damaged phase A windings, it is possible to observe speed oscillations caused by its switching transition between three possible states. These oscillation are caused by two factors. First one is the electrical modification described by (2) and (3). Then the back-EMF modification described in (6). Considering the electrical and controller dynamics, circulating current tend to remain constant for a short transition phase, with a resultant torque respectively higher if the A winding is turned OFF and lower if it is turned ON from idle.

5 ROTOR ECCENTRICITY OUTPUT ANALYSES

The main hypothesis for static rotor eccentricity (RE) simulations is the unbalance direction, fixed in the middle of one A-phase winding (as shown in Fig. 3). This assumption reduces the number of variables to considerate to the measure described in (4). The same computation described in (7) is performed in this case, leading to analogous results. In this case, speed oscillations are caused only by back-EMF modification, and presents more discontinuities around the revolution. Moreover, back-EMF is proportional to rotor speed, causing a rise in total load applied to the stator circuit. Differently from the aforesaid turn-to-turn coil short circuit (SC) case, this damage involves all phases in different manner, determined by the eccentricity direction fixed previously.

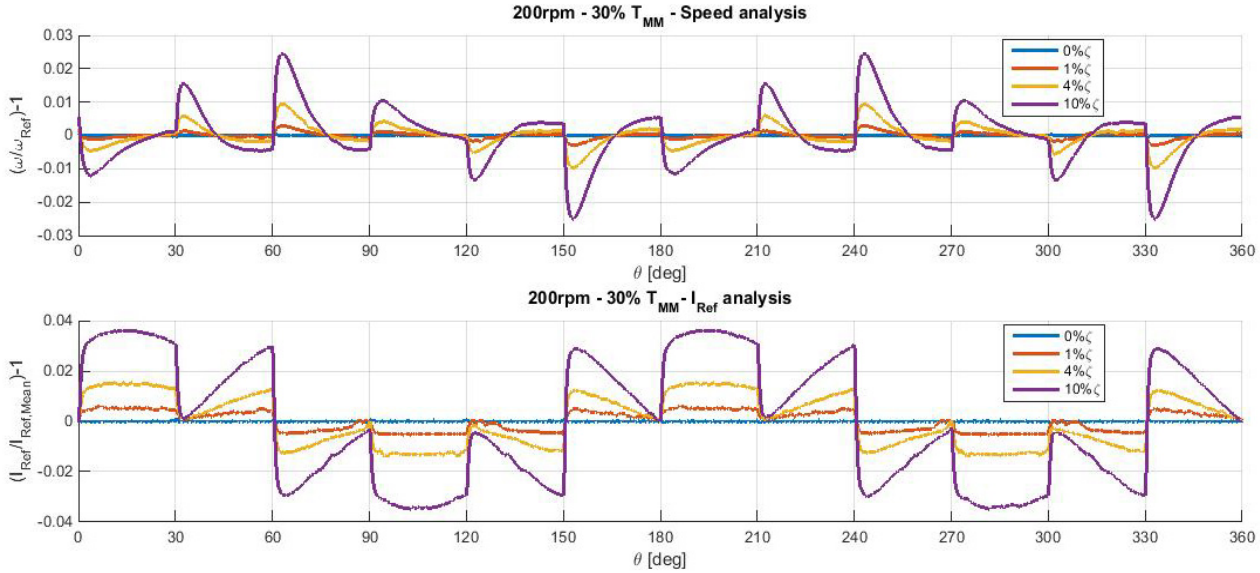

Figure 7 Speed and reference signal response at various RE conditions.

6 DATA PRE-PROCESSING

In order to reduce input data size without losing main signal features, the average value over a 30° interval, corresponding to a single winding coverage, is computed for speed and reference signal:

$$X_{30,i} = \frac{\int_{\theta_i}^{\theta_i+30} X(\theta)\, d\theta}{30} \qquad 1 \leq i \leq 12 \tag{8}$$

Recalling (7), signals are then normalised, and an entire revolution can be represented by twelve significant points corresponding to the windings. One further step is the computation of RMS value over the twelve normalised:

$$X_{RMS} = \sqrt{\frac{\sum_{i=1}^{12} \left(\hat{X}_i\right)^2}{12}} \tag{9}$$

At this point is possible to build the neural network input vector, composed by the working condition by the mean of speed and reference current average values over a revolution and the RMS values representative of the oscillation magnitude:

$$X_{NN} = \begin{bmatrix} \omega_{360} \\ I_{360} \\ \omega_{RMS} \\ I_{RMS} \end{bmatrix} \tag{10}$$

7 NEURAL NETWORK ARCHITECTURE

Characteristic periodic behaviour of speed and reference current can lead to a damage classification by the mean of a *Pattern recognition* network [13]. By the means of one *tansig* hidden layer followed by a *competitive* layer permits to classify input vectors in user-defined classes.

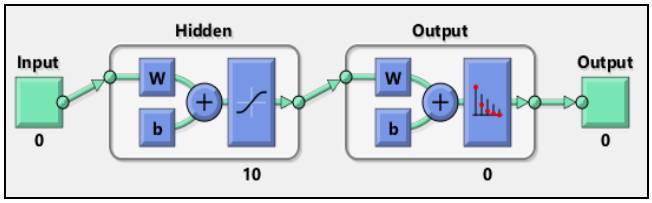

Figure 8 Pattern recognition network.

The *Pattern-recognition* output vectors as per their nature, resolves a nominal classification problem. Considering the fault effects on rotor speed and reference current signal, at different speed and torque conditions, it is not possible to develop a deterministic model, due to the underlying mechanical and electro-magnetic effects. *Tansig* layer is a continuous function, limited between -1 and +1. Its main features is to mitigate values far from origin, highlighting differences between values lying around zero. This fits well the normalisation process performed ahead the network

input. Hence damage classification becomes a stochastic problem, which can be modelled as a *Multinomial Logistic Regression*, performed by a *softmax* layer:

$$\sigma(z)_i = \frac{e^{z_i}}{\sum_{k=1}^{N} e^{z_k}} \tag{11}$$

$$\sum_{i=1}^{N} \sigma_i = 1 \tag{12}$$

This function normalises an input real values-composed vector into a same-size vector which elements sum results one. Under the hypotheses of input data statistic independence, which is satisfied by (10), it is possible to discretize the damage entity in numbered classes.
The output of this layer represents so a probability distribution, where the emerging class is considered for final classification.

7.1 TRAINING PHASE

For every point in Figure 4 several simulations with different failures are performed. The considered damage entity are represented by the following vectors:

$$N_{ph} = [100 \quad 99 \quad 97 \quad 95 \quad 90 \quad 85 \quad 80 \quad 75]_8\% \tag{13}$$

$$\zeta = [0 \quad 1 \quad \dots \quad 10]_{11}\% \tag{14}$$

As eight SC and eleven RE cases are simulated, target sequences are represented by identity matrices respectively of 8 and 11 dimension. Back propagation algorithm is used to train all networks developed.. The scaled conjugate gradient algorithm is used to calculate derivatives of performance with respect to the weight and bias variables. It is based on conjugate directions, and does not perform a line search at each iteration [14]. To assure network generalisation input / target sequence is presented randomly to the training algorithm, as weights and biases initialization.

8 CLASSIFICATION ACCURACY

To evaluate the resultant classification accuracy, confusion matrices is considered. These presents target classes coming from its relative matrix on the x-axis and the related network output, after training phase is conducted. Well classified samples lays on the main diagonal, where target and output corresponds.
In Figure 9, the first row represents normal condition output class (*undamaged*). Every sample out from the first box represents an undetected damage. Considering the #2 and #3 classes (99% and 97% N_{ph} respectively), in which undetected failures occurs, it is possible to states the network sensitivity to SC. Maintaining the input matrix, it is possible to build several target matrices to perform different kinds of classifications. One trivial solution tried is to divide samples into two main categories: normal and damaged condition.

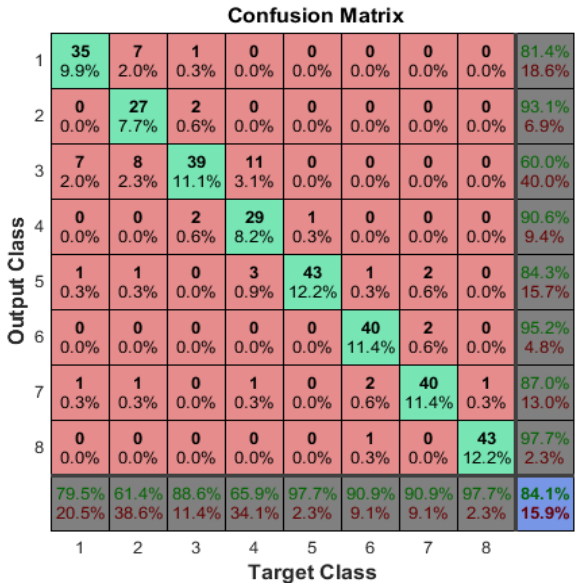

Figure 9 SC confusion matrix.

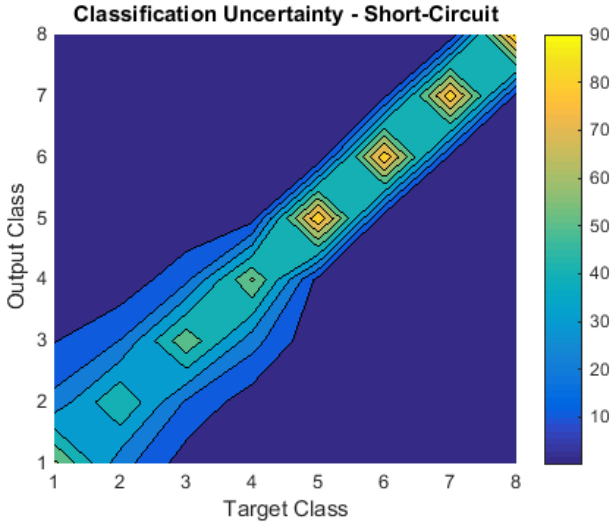

Figure 10 SC Accuracy map.

As the number of considered classes decreases, the classification performance generally rises, as demonstrated in [15]. Analogous results are reached in RE case, proving the method reliability. Taking advantage of the stochastic nature of *softmax* output, it is possible to transform the discrete classification results into a continuous map. By the processing of every network output it is possible to evaluate an overall accuracy as showed in Figure 10. As per the confusion matrix, the main diagonal indicates the well classified elements. Considering the simulated failures vector (13), the higher accuracy occurs for major damages, which are also well distinguished from the adjacent classes, due to the major damage entity gap (1% between classes #1 and #2 – 15% between #7 and #8).

9 MULTIPLE FAILURES

To test the robustness of the designed networks, a multiple failures simulation campaign is performed. Considering the increasing size of the problem, a fixed value of 5%T_{MM} output torque is demanded, with the following *unbalance-short-circuit* combinations considered:

$$\zeta_{\%} = [0 \quad 5 \quad 15]\% \tag{15}$$

$$SC_{\%} = [0 \quad 10 \quad 25]\% \tag{16}$$

As per the architecture and training samples, which considers RMS and averaged values, most of the damage combinations could lead to false positives detection for both damages[15].

9.1 MULTIPLE FAILURES NETWORK

A different approach is followed to develop an additional ANN, which is capable to distinguish the type of failure. *Pattern recognition* networks results the most suitable architecture also in this case. Despite taking advantage of RMS values, which is a scalar measure of oscillation entity, the oscillation shape around an entire revolution is considered. It must be noted that the normalisation process remains the same previously described in (7).

Differently from previous networks, the input vector is composed by the revolution-average values and the sorted vectors of $\hat{X}_{30,i}$ values of speed and *Iref*:

$$X_{rev} = \begin{bmatrix} \hat{X}_{30.1} \\ \vdots \\ \hat{X}_{30.12} \end{bmatrix}_{12\times 1} \tag{17}$$

$$X_{NN} = \begin{bmatrix} \omega_{rev12\times 1} \\ I_{rev12\times 1} \\ \omega_{360} \\ I_{360} \end{bmatrix} \tag{18}$$

The purpose of this network is to recognize oscillation features of different failures combinations trough the analyses of twelve significant points representative of the entire rotation. Also target building has got different purpose. In fact, three classes compose the target vector. Two over three represents the SC and RE failure. The third class is called *interference* class (INT): its purpose is to mitigate the inactive failure probability in the output vector and distinguish also the normal working condition:

$$T_i = \begin{bmatrix} SC \\ INT \\ RE \end{bmatrix} \tag{19}$$

When just one kind of failure is active, relative target vector will contain both the relative failure class and the interference class with a value limited to 0.5 in order to lead the network output and weight modification toward the right class during training phase. The considered target vector and resultant classification lead to a different analysis of results. For this network the confusion matrix cannot highlights the classification performance.

As nine damage combinations are simulated for every speed condition, it is possible to observe the classification results for every combination by pie charts.

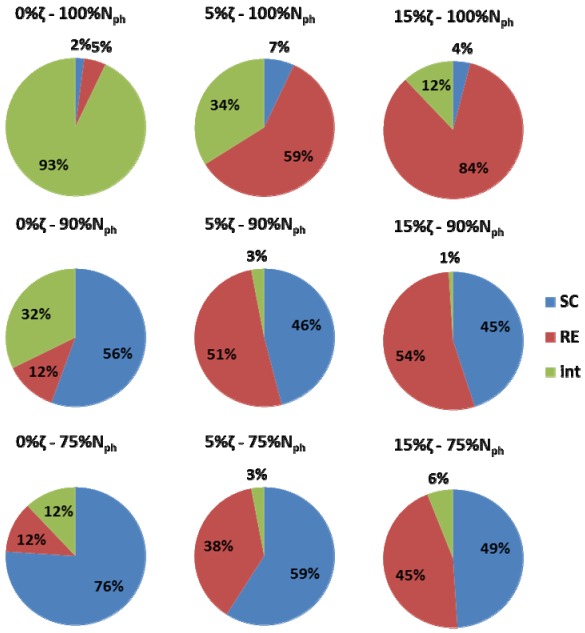

Figure 11 Multiple-failures network accuracy map.

10 CONCLUSIONS

Considering the reduced number and size of inputs, the limited data pre-processing and simple network architecture, the overall classification performance results satisfactory. Fault design is an approximation, not considering the complete electro-magnetic interactions between stator and rotor. Considering the limited failure entity and the low torques and currents involved, hypotheses results acceptable. In fact, the major result is the detection through mechanical and logical signals (shaft speed and Controller Reference current), neglecting electrical signals as phase currents or voltages. Advantages of this approach consists in a limited sensor data demand (i.e. shaft position and Brushless DC motor controller output), which are also cleaner in noise more available respect to electrical measures (e.g. phase voltages and currents). The need of Controller output signal binds the network training to the overall actuation system. This means that the solution shall be characterized for further applications. Interesting developments can be found investigating network suitability in other kinds of actuators. In fact, primary FCS can be considered as speed-position drives where components are not subject to constant stresses and usually works in transitory rather than steady conditions. Other applications like torque motors or pumps concerns significant torques and currents and can work in steady conditions, simplifying the actuator characterization and prognostic work.

REFERENCES

[1] Maggiore P., Dalla Vedova M.D.L., Pace L., Desando A., Proposal of fault analysis parametric method applied to an electro mechanical servomechanisms affected by failures. *International Journal of Prognostics and Health Management*, Vol. 6, No. 1, 2015. ISSN: 2153-2648

[2] Çunkas M., Aydoğdu O., Realization of Fuzzy Logic Controlled Brushless DC Motor Drives using Matlab/Simulink. *Mathematical and Computational Applications*, Vol. 15, pp. 218-229, 2010.

[3] Halvaei Niasar A., Moghbelli H., Vahedi A., Modelling, Simulation and Implementation of Four-Switch Brushless DC Motor Drive Based On Switching Functions. *IEEE EUROCON 2009*, St. Petersburg, pp. 682 -687, 2009.

[4] Lee B.K., Ehsani M., Advanced Simulation Model for Brushless DC Motor Drives. *Electric Power Components and Systems*, Vol. 31, No. 9, pp. 841-868, 2003. ISSN: 1532-5008

[5] Hemanand T., Rajesh T., Speed Control of Brushless DC Motor Drive Employing Hard Chopping PWM Technique Using DSP. *Proceedings of India Intern. Conference on Power Electronics (IICPE 2006),* 2006.

[6] Haskew T.A., Schinstock D.E., Waldrep E., Two-Phase On' Drive Operation in a Permanent Magnet Synchronous Machine Electromechanical Actuator. *IEEE Trans. on Energy Conversion*, Vol. 14, No. 2, 1999.

[7] Borello L., Villero G., Dalla Vedova M.D.L., New asymmetry monitoring techniques: effects on attitude control. *Aerospace Science and Technology*, Vol. 13, No. 8, pp. 475-487, 2009.

[8] Borello L., Dalla Vedova M.D.L., Jacazio G., Sorli M., A Prognostic Model for Electrohydraulic Servovalves. *Annual Conference of the Prognostics and Health Management Society*, San Diego, CA, 2009.

[9] Borello L., Dalla Vedova M.D.L., A dry friction model and robust computational algorithm for reversible or irreversible motion transmission. *International Journal of Mechanics and Control*, Vol. 13, No. 2, pp. 37-4, 2012.

[10] Farooq J.A., Djerdir A., Miraoui A., Modelling and simulation of stator winding inter-turn faults in permanent magnet synchronous motors. *COMPEL - The International Journal for Computation and Mathematics in Electrical and Electronic Engineering*, Vol. 27, No. 4, pp. 887–896, 2008. ISSN: 0332-1649

[11] Kim B.W., Kim K.T., Hur J., Simplified impedance modeling and analysis for inter-turn fault of IPM-type BLDC motor. *Journal of Power Electronics*, Vol. 12, pp. 10-18, 2012. ISSN: 1598-2092

[12] Dalla Vedova M.D.L., Maggiore P., Pace L., Romeo S., Proposal of a model based fault identification neural technique for more-electric aircraft flight control EM actuators. *WSEAS Transactions on Systems*, Vol. 15, Art. #3, pp. 19-27, 2016.

[13] Chopra I., Ganguli R., Haas D.J, Detection of Helicopter Rotor System Simulated Faults Using Neural Networks. *Proceedings of the 37th Structures, Structural Dynamics and Materials Conference (AIAA-96-1646-CP)*, Salt Lake City, UT, pp. 1246-1263, 1996.

[14] Møller M.F., A scaled conjugate gradient algorithm for fast supervised learning. *Neural networks*, Vol. 6, No. 4, pp. 525-533, 1993.

[15] De Fano D., *Artificial Neural Network design for BLDC Motor short circuit and rotor unbalance early detection*. MSc Thesis, Politecnico di Torino, 2016.